ELEMENTA
Science of the Anthropocene

Gillard, B, et al. 2019. Physical and hydrodynamic properties of deep sea mining-generated, abyssal sediment plumes in the Clarion Clipperton Fracture Zone (eastern-central Pacific). *Elem Sci Anth*, 7: 5. DOI: https://doi.org/10.1525/elementa.343

RESEARCH ARTICLE

Physical and hydrodynamic properties of deep sea mining-generated, abyssal sediment plumes in the Clarion Clipperton Fracture Zone (eastern-central Pacific)

Benjamin Gillard[*,†], Kaveh Purkiani[*], Damianos Chatzievangelou[†], Annemiek Vink[‡], Morten H. Iversen[*] and Laurenz Thomsen[†]

The anthropogenic impact of polymetallic nodule harvesting in the Clarion-Clipperton Fracture Zone is expected to strongly affect the benthic ecosystem. To predict the long-term, industrial-scale impact of nodule mining on the deep-sea environment and to improve the reliability of the sediment plume model, information about the specific characteristics of deep-sea particles is needed. Discharge simulations of mining-related fine-grained (median diameter ≈ 20 µm) sediment plumes at concentrations of 35–500 mg L^{-1} (dry weight) showed a propensity for rapid flocculation within 10 to 135 min, resulting in the formation of large aggregates up to 1100 µm in diameter. The results indicated that the discharge of elevated plume concentrations (500 mg L^{-1}) under an increased shear rate ($G \geq 2.4\ s^{-1}$) would result in improved efficiency of sediment flocculation. Furthermore, particle transport model results suggested that even under typical deep-sea flow conditions ($G \approx 0.1\ s^{-1}$), rapid deposition of particles could be expected, which would restrict heavy sediment blanketing (several centimeters) to a smaller fall-out area near the source, unless subsequent flow events resuspended the sediments. Planning for in situ tests of these model projections is underway.

Keywords: Deep-sea mining; Sediment plume; Particle size; Aggregation; Settling velocity

Introduction

Over the past decade, increasing global consumption and rising market prices of metals, together with technological improvements, have driven several countries and industries to prospect the deep-sea environment for mineral resources, including polymetallic nodules (Hein and Koschinsky, 2013). Polymetallic nodules that are rich in metals and rare earth elements lie on the surface of the abyssal sediment. The Clarion-Clipperton Fracture Zone (CCZ), located in the northeastern equatorial Pacific Ocean (**Figure 1**), contains the most extensive nodule deposition known (Halbach and Fellerer, 1980) and is of high economic interest (Wedding et al., 2015). However, nodule fields are also essential habitats for benthic communities (Kaiser et al., 2017), and more than half of the megafauna discovered in the CCZ rely on the nodules as a hard substrate (Amon et al., 2016).

The potential future use of mining equipment on the ocean floor and the subsequent return of mining products (e.g., sediment, water, and abraded nodule debris) to the benthic boundary layer (BBL) would create an operational and discharge plume of fine particulate material (Oebius et al., 2001). Sediment redeposition and bottom blanketing within the vicinity of the mining site ("near field") could potentially bury benthic organisms, clog the respiratory surfaces of filter feeders and pollute the food supply for most benthic organisms. Potential long-range, lateral and vertical dispersion of fine-grained plume particles would have a lower impact but is expected to spread over several hundreds of kilometers from the disturbance location ("far field"). Both processes would affect the deep-sea ecosystem structure and functioning to a certain, although presently unknown, extent (Ramirez-Llodra et al., 2011).

To date, few studies have analyzed the hydrodynamic behavior of original plume particles and modeled the scale of the impact at different temporal and spatial scales in the benthic boundary layer (Aleynik et al., 2017; Jones et al., 2017). Multiple local and regional factors, such as the physical and chemical properties of the bottom sediments, the hydrodynamic regime (near and far field), bottom topography and the type of mining equipment, must be considered simultaneously. Plume modeling of two small-scale benthic impact experiments carried out

* MARUM – Center for Marine Environmental Sciences, University of Bremen, Bremen, DE

† Jacobs University, Bremen, DE

‡ BGR, Bundesanstalt für Geowissenschaften und Rohstoffe, Hannover, DE

Corresponding author: Benjamin Gillard (b.gillard@jacobs-university.de)

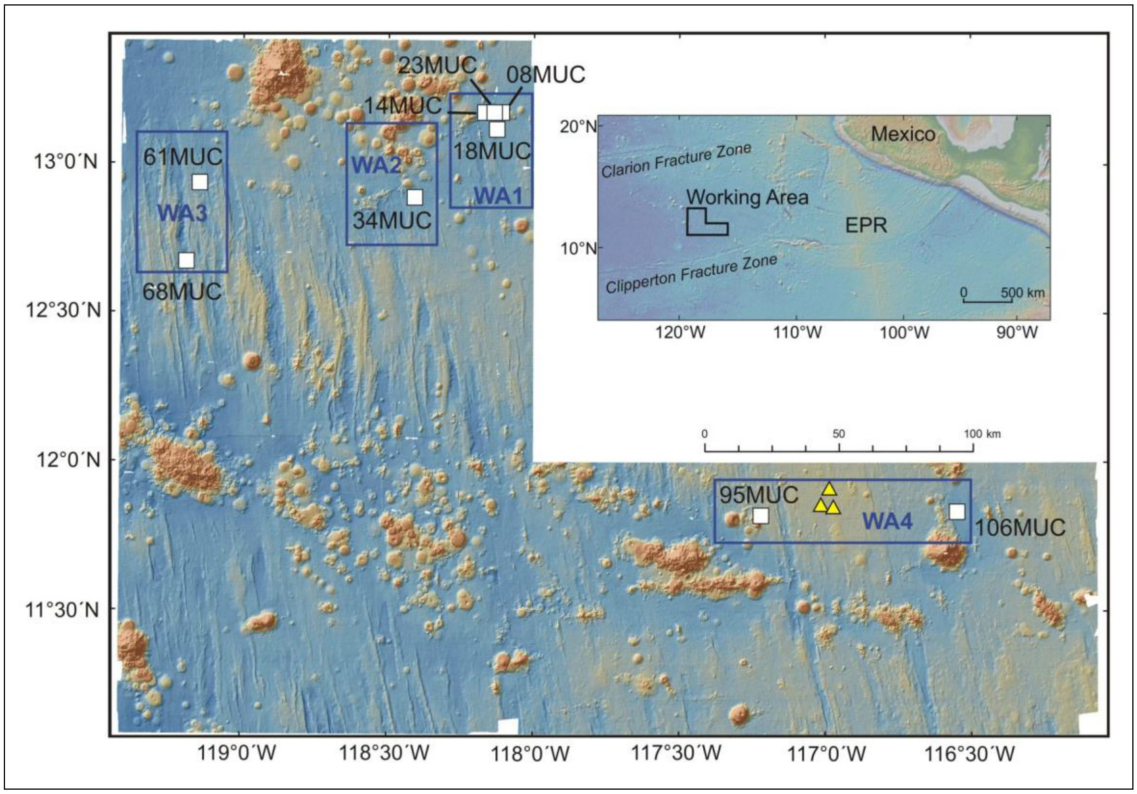

Figure 1: Study areas and locations of sediment samples in relation to the topography. The area is located in the eastern German polymetallic nodule license area in the northeastern Pacific Ocean and is characterized by numerous seamounts, NW-SE ridge systems and flat abyssal plains. Blue rectangles encompass the working areas WA1 to WA4 of cruise SO-240 (Kuhn, 2015). White squares represent locations of sediment core sampling by multicorer (MUC). Yellow triangles represent the position of three acoustic current meters that recorded current speeds and directions close to the seafloor throughout three consecutive years. Inset: view of the license area in relation to the East Pacific Rise (EPR) and the Clarion and Clipperton fractures. DOI: https://doi.org/10.1525/elementa.343.f1

in the 1990s (discharge of ca. 10 kg s^{-1} along predefined tracks) showed that 90% of the suspended particles created by artificial disturbance of the seafloor settled within a radius of 2 km from the disturbance area (Fukushima, 1995; Nakata et al., 1997).

Recent modeling of an industrial-scale, near-bottom sediment plume in the case study area in the CCZ with a discharge rate of 280 kg s^{-1} indicated that more than 50% of the suspended particles would settle within several kilometers of the source region within 10 days. The remaining particles were transported outside the model boundaries (Aleynik et al., 2017). However, the cohesive properties, aggregation potential and different settling processes of fine-grained deep-sea sediments were not considered, even though they have a considerable effect on plume sediment deposition. We believe that the use of site-specific information about particle behavior under different plume concentrations, in combination with high-resolution bathymetric and oceanographic data, will aid greatly in the initialization and calibration of existing sediment transport models for the nodule fields of the CCZ.

To provide more insight into the likely behavior of the sediment plume produced by an industrial-scale mining operation, our research aims were to (1) produce a complete set of sedimentological parameters that are crucial for model reliability and accuracy and (2) discuss the optimal discharge release conditions that could result in a lower impact on the environment. For these purposes, laboratory experiments and particle transport modeling were carried out using abyssal sediments from the CCZ and simulating the *in-situ* conditions encountered there.

Materials and methods

Sampling site and oceanographic data acquisition

Surface sediment samples were obtained with a multicorer (MUC) from nine locations within the eastern German license area for the exploration of polymetallic nodules in the CCZ (RV *Sonne* Cruise SO-240 (Kuhn, 2015); see **Figure 1** and Table S1 for details and exact locations). The eastern boundary of the license area, which totals 56,000 km^2, is located approximately 2500 km west of Mexico. The predominantly fine-grained sediments derive from different topographic environments at water depths of ~4300 m, including flat abyssal plains, NW–SE trending ridge systems and the rise of seamounts. The top 10 cm of sediment from one multicore per location were sampled at 1-cm intervals for detailed sedimentological analysis. Long-term data on speed and direction of current, as well as background turbidity close to the seafloor, were obtained from three moorings deployed in the eastern part of the license area (yellow triangles in **Figure 1**) throughout three consecutive years, from April 2013 to

May 2016. An upward-looking 600 kHz acoustic doppler current profiler (ADCP) was measured at hourly intervals during the first year and then at 45-min intervals during the next two years. High-quality data were retrieved for the water mass 15–20 m above the seafloor (Kuhn, 2015).

Experimental conditions

All experiments were conducted in a temperature-controlled cool container in triplicate to account for random experimental error and to facilitate the posterior statistical treatment. *In-situ* temperature and salinity (1.5°C and 34.68) were reproduced and filtered (0.2 μm) artificial seawater was used.

Sediment particle size distribution

Particle size distribution of suspended sediment was measured using the combined approach of the high-resolution Digital Floc Camera (DFC) and the LISST-100X type C (Mikkelsen et al., 2005; Hill et al., 2011). Detection of particles with the floc camera was inspired by Sternberg et al. (1996). These techniques were applied to use a non-destructive technique on untreated suspended sediments and to apply *in-situ* and *ex-situ* technologies for a realistic comparison with the impact assessment of future mining activities.

The suspension was first analyzed with the LISST-100X (60 measurements at 1 Hz) and then transferred into the viewing chamber of the floc camera for image analysis. The resulting particle volume distributions from both instruments were compared in the overlapping detection range (10 size classes ranging from 66.9 to 381 μm). A correction was applied based on the linear relationship between the volume concentrations detected by the two instruments. The subsequent merging procedure resulted in a size distribution ranging from 1.9 μm to several millimeters. As in Mikkelsen et al. (2005), the correction was used only to scale between the instruments, and did not affect the shape of the size distribution. Instruments details, linear coefficients and experimental protocols are provided in Figure S1, Tables S2 and S3 and Text S1.

The deep-sea sediment aggregation process

Aggregation due to differential settling

The propensity of deep-sea sediment (inorganic and organic material) in suspension to form aggregates over time under conditions of differential settling (the zero shear rate) was assessed using roller tank incubations (Lick et al., 1993; Iversen et al., 2010). Each vessel consisted of a 1.15 L Plexiglas cylinder that was rotated on its side at a fixed angular velocity to reach solid body rotation, providing a continuous settling environment. The hydrodynamics of the system were characterized by Jackson (2015). Four sediment concentrations (35, 105, 175 and 500 mg L^{-1}) were prepared from a stock solution of 5 g L^{-1}. The suspension was first analyzed with the LISST-100X (60 measurements at 1 Hz), then introduced into the roller tank and rotated at a fixed rate of 3 rpm. The formation of aggregates was observed with the camera over time. For every measurement, a horizontal particle camera transect from the center to the outer rim of the roller tank was performed to ensure a complete view inside the cylinder. To prevent disproportionate aggregation due to the recirculation of settled aggregates in the vessel, the experiment was stopped when the first aggregates reached the bottom of the rotating roller tank. After several minutes, when all the aggregates had settled to the bottom, the supernatant was reanalyzed with the LISST-100X.

Aggregation due to turbulent shear

The effect of the shear rate on the aggregation behavior of plume particles (inorganic and organic material) was investigated in a horizontal Couette reactor (Drapeau et al., 1994). The chamber consisted of a fixed inner cylinder and an outer rotating cylinder. Depending on the angular velocity of the outer cylinder, a variable shear flow regime can be produced. A detailed description of the chamber is provided in Figure S2. The calculation of the mean shear rate G (s^{-1}) produced in the chamber followed Van Duuren's (1968) method. The Couette flow reactor was used instead of other mixing devices, such as an oscillating grid or paddle mixer, because of the uniformity of the produced turbulent shear flow and the absence of mixing mechanisms that prevent aggregate breakup during mixing (Coufort et al., 2005; Serra et al., 2008; Zhu et al., 2016). Each experimental approach has limitations but as Serra et al. (2008) concluded, the Couette reactor is still the most suitable method for aggregating particles without interference. The results also followed the same trends as experiments conducted inside a 1,000 L water column simulator (Porter et al., 2004).

Three sediment plume concentrations (105, 175 and 500 mg L^{-1}) were prepared from the stock solution. The suspension was first analyzed with the LISST-100X (60 measurements at 1 Hz), then introduced into the Couette reactor and rotated under three different shear rates (2.4, 5.7 and 10.4 s^{-1}). The shear rates of 0–10.4 s^{-1} were used to simulate a broad spectrum of expected flow conditions during mining operations: from very slow deep-sea currents via "passing eddies" to elevated turbulence intensities behind the collector and exhaust pipe of mining vehicles. Floc aggregation was observed with the camera over time. As with aggregation due to differential settling, the experiment was stopped when the first aggregates reached the bottom of the chamber. After several minutes, when all of the aggregates had settled to the bottom, the remaining water was reanalyzed for particle size distribution using the LISST-100X.

Settling velocity

For the assessment of the sinking velocities of aggregates vs. particle size, a custom settling column was built. The conceptual design was inspired by a combination of the settling column of the LISST-STX (Agrawal and Pottsmith, 2000) and the square cross-section cylinder (Thomsen and Gust, 2000) used for camera analysis. A detailed description of the settling column and sample preparation is given in Figure S3 and Text S1.

Aggregates from the flocculation chambers were carefully transferred into a settling tube by settling/sliding them along the walls of the flocculation chambers into

the next experimental chamber. This approach is similar to the process that occurs inside *in-situ* particle cameras or water column simulators (Sternberg et al., 1999; Porter et al., 2004). The aim was to characterize the general size and settling relationship (Lick et al., 1993; Manning and Dyer, 1999) and erosion behavior of these aggregates (Thomsen and Gust, 2000; Thomsen et al., 2002) for subsequent numerical plume modeling of varying particle size classes. The particle sinking velocities were measured with the camera at the lower end of the column, allowing the aggregates to reach their terminal settling velocities before video analyses were conducted (Nowald et al., 2009).

Bedload transport and critical shear velocity (u_{*cri})

Bedload transport and critical shear velocity (u_{*cri}) were determined in a Gust erosion chamber with a diameter of 20 cm, with controlled bottom shear stress (Thomsen and Gust, 2000). Aggregates were carefully transferred from the flocculation reactor to the erosion chamber (see the method described above for the settling velocity). The u_{*cri} was increased incrementally in steps of 0.1 cm s^{-1} every 5 min until u_{*cri} was attained, and the aggregates were resuspended (Pabortsava et al., 2011).

Modeling of sediment plume dispersion

A three-dimensional numerical ocean model was developed to assess the application of the experimental results in a realistic scenario and predict the sediment transport at the study site. The numerical simulations were carried out using the Massachusetts Institute of Technology general circulation model (MIT GCM; Marshall et al., 1997). No-slip conditions at the lateral and bottom boundaries were applied. The initial values of the horizontal and vertical diffusivities of every tracer were set to 0.1 and 10^{-4} m^2 s^{-1}, respectively. However, the model uses the parameterization method of Klymak and Legg (2010) to obtain suitable eddy viscosity and turbulence dissipation values.

A multiple one-way nesting approach was applied. The coarsest model (3600 m horizontal resolution) was laterally forced by the seawater properties. The zonal and meridional current velocities were extracted from the Hybrid Coordinate Ocean Model (HYCOM). For the following higher resolution configuration (1000 m, 300 m), the lateral boundary conditions were supplied by the previous coarser model to a final horizontal resolution of 150 m and a vertical resolution of 5 m.

The model domain was located in the CCZ German license area (**Figure 1**), where a collector vehicle trial is being planned for early 2019. A flat ocean bottom at a water depth of 4200 m was assumed for simplicity. Sediment transport was simulated by solving the passive tracer equation with an additional settling velocity and sediment source for each sediment class. The sediment transport equation (Equation 1) is written as:

$$\frac{\partial c}{\partial t}+u\frac{\partial c}{\partial x}+v\frac{\partial c}{\partial y}+w\frac{\partial c}{\partial z}+\frac{\partial (w_s c)}{\partial z}=\frac{\partial}{\partial x}\left(\nu_x\frac{\partial c}{\partial x}\right)+\frac{\partial}{\partial y}\left(\nu_y\frac{\partial c}{\partial y}\right)+\frac{\partial}{\partial z}\left(\nu_z\frac{\partial c}{\partial z}\right)+q_s \quad \text{(Eq. 1)}$$

where c is the sediment concentration; u, v, and w are the velocity fields, w_s is the settling velocity; ν_x, ν_y, and ν_z are the horizontal diffusivity coefficients; and q_s is the source term. The settling velocities of the sediment particles were directly employed from the results of the experimental analysis considering the natural conditions of the seawater, sediment properties and flocculation processes. Based on data provided by the manufacturer of the collector vehicle, the sediment discharge was set at a rate of 60 t h^{-1} for a period of 4 days at 5 m above the seafloor, with the collector vehicle moving at a constant velocity of 0.5 m s^{-1} in an area 300 m by 300 m. The current model grid resolution (150 × 150 × 5 m) was not high enough to simulate a water swirl exerted by a moving underwater collector (which would require higher computational cost and time). Therefore, the turbulence induced by the nodule collector and the effect of the initial momentum of the collector's exhaust on the movement of sediment particles was mimicked with a higher shear rate (G = 2.4), which was at least one order of magnitude higher than the expected shear rate of the ambient flow in the deep ocean in this area.

Sediment deposition under deep ocean hydrodynamic conditions was investigated under two benthic flow scenarios: (1) a collector discharge concentration of 500 mg dw L^{-1} under typical average flow conditions of 3.8 cm s^{-1} and a predominantly easterly flow (aggregate dataset G = 0) and (2) a collector discharge concentration of 500 mg dw L^{-1}, followed by a remaining plume concentration of 105 mg dw L^{-1} during a simulated passage of an eddy under a northeasterly flow of >10 cm s^{-1} (aggregate dataset G = 2.4).

Image treatment analysis

Values for the particle size, shape descriptor factors (i.e., circularity, roundness and solidity) and settling velocities were obtained using FIJI software (v.1.51n); steps for processing raw images were adapted from Shen (2016) as follows. The BIOVOXXEL toolbox macro was used to evaluate the sensitivity of the thresholding technique, resulting in the automatic "Intermode" thresholding algorithm being selected as the most accurate for the dataset. Out-of-focus particles were removed manually. Particle settling velocities were determined using the FIJI plugin TrackMate. A stack of pictures was first preprocessed, and the plugin was run with binary images. Every track was visually evaluated, and a minimum of three time points per track was required to validate the track. The average settling speed was converted to m d^{-1} velocity.

Statistical analysis

Statistical analysis was performed in R (R Core Team, 2016). The particle size and settling velocity datasets were first cleaned of extreme outliers (i.e., values higher and lower than 1.5 interquartile ranges above and below the 0.75 and 0.25 quartiles, respectively) and grouped by sediment concentration (105, 175 and 500 mg L^{-1}) and by shear rate (0, 2.4, 5.7 and 10.4 s^{-1}). As the particle sizes differed among the different groups, the measured velocities were normalized to the median particle size. Kruskal-Wallis rank sum tests, followed by pairwise Dunn's tests with Bonferroni correction, were performed on the normalized settling velocities.

Modeling of settling velocities

A non-linear (logistic-sigmoidal) curve was fitted to model the settling velocity against the particle size for each concentration-shear rate combination, and 95% confidence and prediction intervals were calculated based on each model. The curves followed Equation 2:

$$y = \frac{a_1}{1 + e^{\frac{a_2 - x}{a_3}}} \qquad \text{(Eq. 2)}$$

where a_1 is the upper asymptotic limit of the curve, a_2 is the inflection point of the curve and a_3 represents the scaling factor for the size axis. All model coefficients and statistical significance levels are provided in detail in Table S4.

Results

Analysis of sediment particle size distribution

The particle size distribution of nine sediment cores from the German polymetallic nodule license area in the CCZ (**Figure 1**) was analyzed. Two regions (i.e., abyssal plain vs. local seamounts and ridges) were found within the four work areas (**Figure 2**).

The sediment size distributions from the abyssal plain environments (MUC samples 14, 18, 23, 34 and 61; median diameter, d_{50} = 20.0 ± 3.1 µm) were characterized by finer grain sizes, with 28, 57 and 15% by volume of the cumulative frequency corresponding to size ranges <10, 10–63 and >64 µm, respectively. All samples exhibited a multimodal distribution, with the 90% inter-percentile range between 3 and 139 µm, a dominant mode in the coarse silts around 20 µm and three weaker ones located at 6, 56 and 252 µm.

In contrast, sediments within the vicinity of the local seamounts and ridges (MUC samples 08, 68, 95 and 106; d_{50} = 33 ± 13 µm) showed a shift toward coarser size fractions, with an average cumulative frequency of 46% by volume in the size range >63 µm. The same multimodal distribution was observed as for the abyssal plain samples, except with a broader inter-percentile range (4 to 273 µm), with modes rising at 56 and 252 µm. The sand fraction was investigated using binoculars and identified as debris of biogenic deposits, including foraminiferal, radiolarian and diatom residues (Figure S4). The descriptive statistical analysis of sediment particle size distribution is provided in Table S5.

The particle aggregation process

Aggregation of plume particles under typical deep-sea flow conditions of a very low shear rate (G ≈ 0 s^{-1}) took longer and resulted in larger plume aggregates (aggregation time, T_a = 45–135 min to reach a median diameter, d_{50} = 850–1100 µm) than that for the aggregates produced under elevated shear rates (G = 2.4–10.4 s^{-1}; T_a = 10–50 min to reach d_{50} = 250–550 µm, as expected during the passage of an eddy or in the wake of a large mining vehicle; **Figure 3A–E**).

In the absence of shear, aggregation increased proportionally with increasing plume concentration (linear slope factor of 0.05; Figure S5). For example, when the initial discharge concentration doubled, the size of the aggregates doubled during the same aggregation duration.

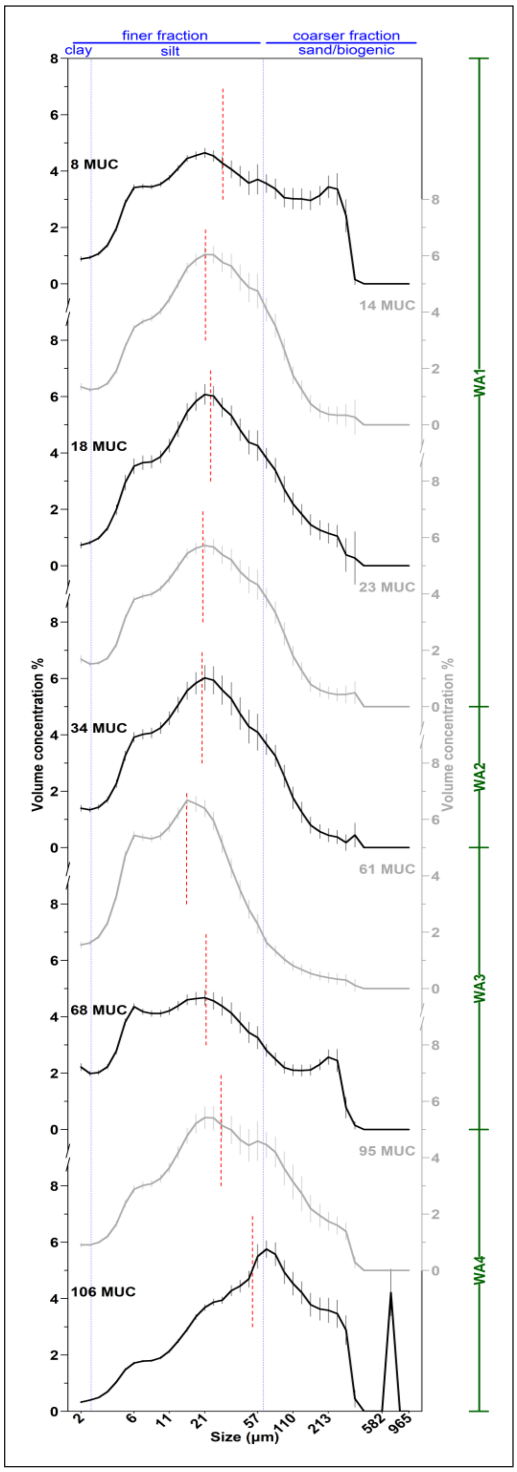

Figure 2: Particle size distribution in the mixed top 10-cm sediment layer. Distributions are expressed as a percentage of the volume concentration obtained from the merged results of the LISST-100X and the floc camera (figure inspired by McCave et al., 1995); vertical dashed red lines indicate the median diameter of the sample distribution; the vertical green line indicates sample location by work area (WA1–4). "Finer fraction" refers to particles <63 µm, including clay (<2.5 µm) and silt (2.5 ≤ x < 63 µm); "coarser fraction" refers to particles ≥63 µm and was identified as a biogenic sediment. Black and gray are used only to aid visualization and do not represent grouping of the samples. DOI: https://doi.org/10.1525/elementa.343.f2

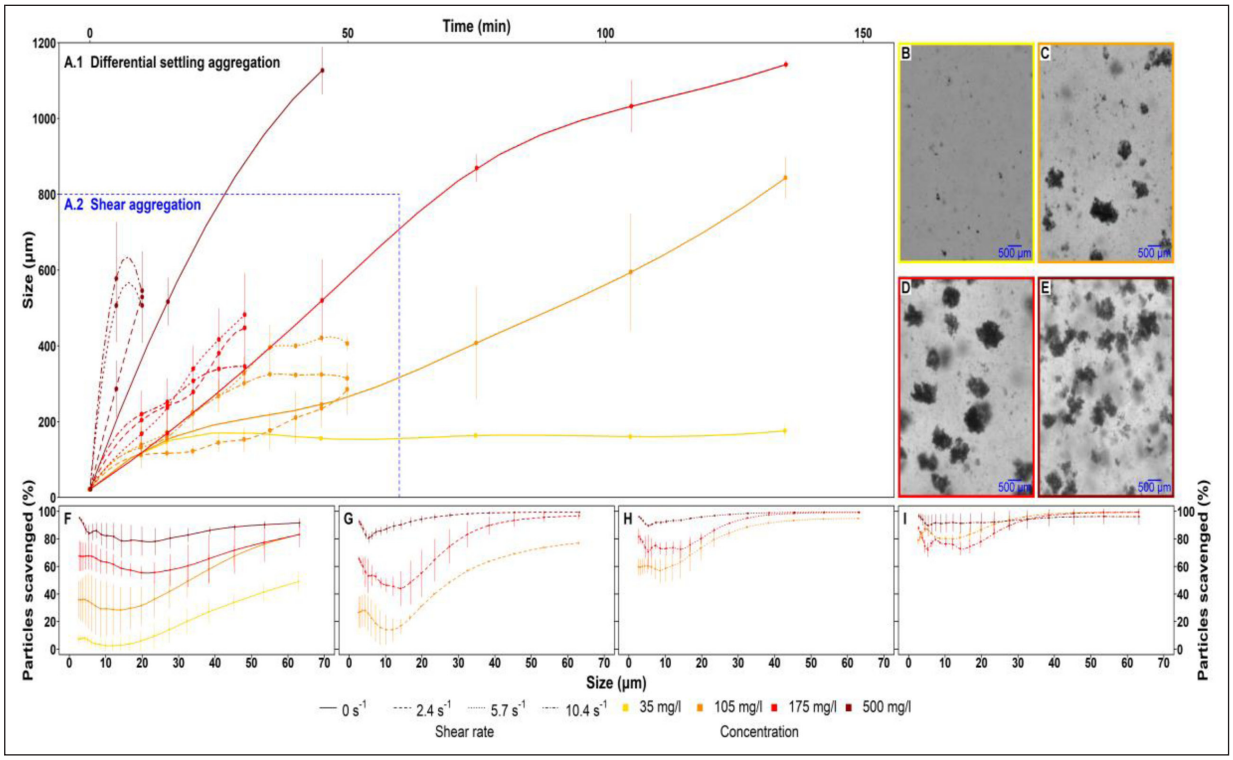

Figure 3: Aggregation propensity of deep-sea sediment. (A) Evolution of median-size flocs produced under different (color-coded) sediment plume concentrations over time, by (A.1) differential settlement aggregation and (A.2) shear aggregation. Pictures of aggregates produced under (color-coded) particle concentrations of **(B)** 35 mg L^{-1}, **(C)** 105 mg L^{-1}, **(D)** 175 mg L^{-1}, and **(E)** 500 mg L^{-1}. Particle size involvement during the process of aggregate formation under different (line dashed) shear rates of **(F)** G = 0 s^{-1}, **(G)** G = 2.4 s^{-1}, **(H)** G = 5.7 s^{-1}, and **(I)** = 10.4 s^{-1}. DOI: https://doi.org/10.1525/elementa.343.f3

At a fixed plume concentration, increasing the shear rate led to 30% more aggregation (**Figure 3A**). At a shear rate of G ≈ 10 s^{-1}, which can be expected behind a fast-moving mining vehicle, the plume flocs revealed a shift toward smaller aggregate sizes, indicating disaggregation. The scavenging of plume particles by already formed aggregates is a function of the concentration of plume particles and the shear rate (**Figure 3F–I**). Thus, by increasing either the plume concentration or the shear rate, we observed faster scavenging by previously formed aggregates (**Figure 3I**).

Settling velocities of aggregated plume particles

The size and settling velocities of flocculated plume particles varied from 70 to 1357 µm and from 7 to 355 m d^{-1}, respectively (**Figure 4**). In general, larger aggregates settled faster than smaller ones. However, the size-specific settling velocities of the formed aggregates depended on the initial sediment plume concentration and the shear rate applied during aggregation (**Figure 4C–D**).

Under G = 0 s^{-1} (i.e., differential settling), the size-specific settling velocities were significantly lower for aggregates formed under large sediment concentrations of 175 mg L^{-1} (Kruskal-Wallis H = 145.3 for 3 df, $p < 0.0001$) when compared to those formed at small concentrations of 35 mg L^{-1} (66.60 m d^{-1} and 143.5 m d^{-1}, respectively; **Figure 4A**). No statistically significant differences in settling velocities (Table S7 for Dunn's pairwise comparisons) were observed at concentrations ≥175 mg L^{-1}. Morphological analysis (circularity, roundness and solidity) of the entire size spectrum, available in Figure S6, revealed that larger plume concentrations resulted in the formation of aggregates that had more complex shapes.

Regardless of the plume concentrations, a moderate shear rate of G = 2.4 s^{-1} during aggregation resulted in elevated size-specific settling velocities (Kruskal-Wallis H = 411.5 for 3 df, $p < 0.0001$, **Figure 4B**; median w_s = 65–103 m d^{-1}). Once the shear rate exceeded 5.7 s^{-1}, no statistically significant differences in the size-specific settling velocities of the aggregates were detected (see Table S8, for Dunn's pairwise comparisons).

To derive additional conclusions about plume behavior, only the 0 G and 2.4 G conditions (representing free-stream velocities of 0 and ≈25 cm s^{-1}) were selected as the model input parameters, as these conditions represent the full spectrum of the expected hydrodynamic *in situ* conditions at the study site. A non-linear (logistic-sigmoidal) curve model was chosen to best fit the behavioral change in the settling velocity against particle size (**Figure 4C–D**). All coefficients, significance levels and model sensitivities are provided in detail in Figure S7 and Table S4.

Critical shear velocities for resuspension of deposited plume aggregates

For the model input, as well as for the calculation of the mass fluxes in the benthic boundary layer, the critical shear velocities required for the resuspension of newly settled plume aggregates were measured in a benthic erosion chamber. The resuspension behavior of aggregates

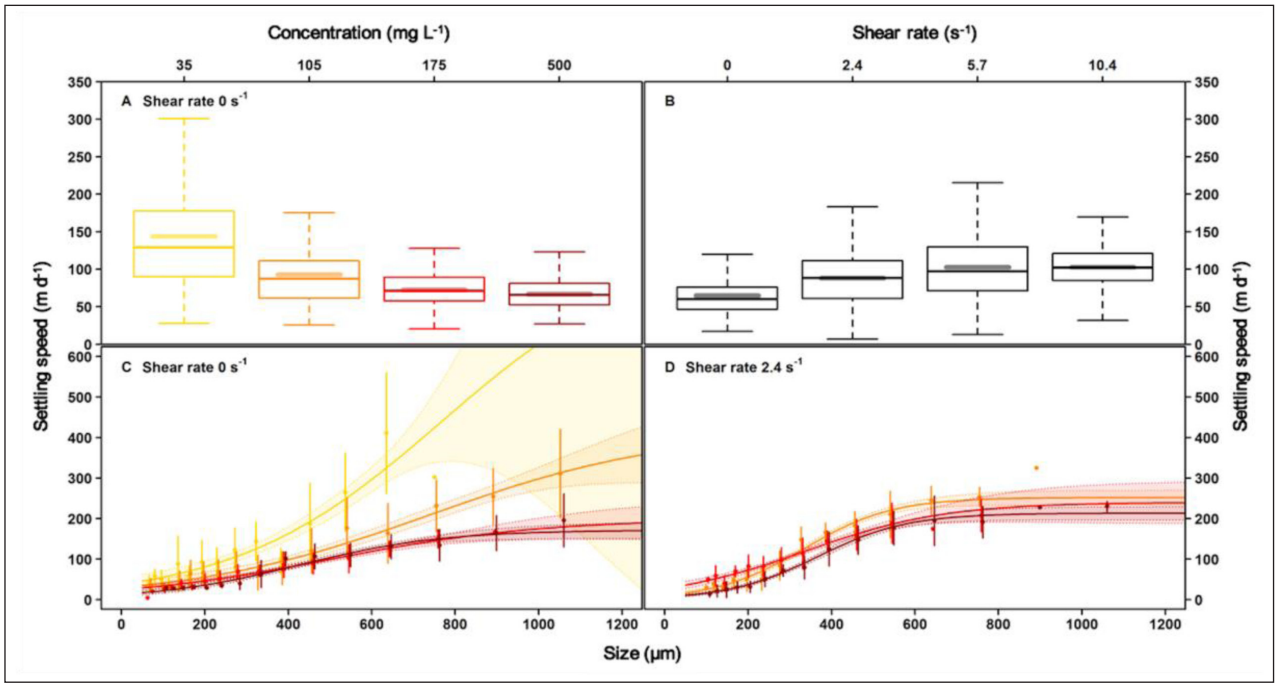

Figure 4: Settling velocity of deep-sea plume aggregates. (A) Boxplots of the settling velocities of aggregates produced under a shear rate of G = 0 s^{-1} under four (color-coded) sediment plume concentrations. **(B)** Boxplots of the settling velocity against the shear rate, for concentrations of 105–500 mg L^{-1}. For a comparison with the treatments in A and B, the settling velocities were normalized to the median particle size. **(C)** Fitted model curves (non-linear logistic-sigmoidal) of the settling velocity against particle size for aggregates produced under a shear rate of G = 0 s^{-1}. (**D**) Fitted model curves (non-linear logistic-sigmoidal) of the settling velocity against particle size for aggregates produced under a shear rate of G = 2.4 s^{-1}. The 95% confidence intervals are depicted for every modeled curve. For visual purposes, size data grouped in the four (color-coded) classes were plotted on the curves. The raw data can be found in Table S6. DOI: https://doi.org/10.1525/elementa.343.f4

under varying plume concentrations did not differ under the 0 G and 2.4 G conditions. A critical shear velocity of u_{*cri} = 0.3 cm s^{-1} corresponding to a bottom current velocity at u_{100} (1 m above the seabed) of ≈4–5 cm s^{-1} was required to initiate bedload transport. Suspended load transport was observed at $u_{*cri} \geq 0.5$ cm s^{-1} (u_{100} = 7–8 cm s^{-1}), when the plume aggregates were resuspended. Full resuspension was observed at $u_{*cri} \geq 0.7$ cm s^{-1} (u_{100} = 9–12 cm s^{-1}).

Sediment plume dispersion modeling

The sediment parameters derived from the analyses were implemented in a hydrodynamic model to predict the plume dispersal and sediment blanketing during and 1 day after a simulated 4-day collector trial that is planned for the German license area in early 2019. The amount of sediment deposition from the plume that was modeled for each of the three particle size classes, d_{25}, d_{50} and d_{75}, is shown in **Figure 5**. Under low flow conditions (G = 0 s^{-1}) a plume blanketing of >0.1 mm extended to a maximum of 2.5 km from the mining site (source 0;0) and thinned out to zero within a maximum distance of 4 km. Under enhanced bottom current velocities, such as those associated with eddy passage (G = 2.4 s^{-1}), the d_{50} and d_{75} coarse fractions settled even more quickly, and a plume deposition of >0.1 mm reached a maximum distance of 3.5 km downstream from the source. However, due to the greater current speeds, the lower aggregation and the subsequent settling speeds of fine particles (d_{25}), only 80% of the plume settled in comparison to 96% under low flow conditions (**Table 1**). The resulting blanketing thinned out to zero 9 km from the mining site.

Table 1: Percentage of suspended particles remaining in the water column at the end of the modeling exercise (5 days after the start of the collector trial) for three particle size classes. DOI: https://doi.org/10.1525/elementa.343.t1

Experiment	Remaining suspended material (%)		
	d_{75}	d_{50}	d_{25}
G = 0 s^{-1}	1.43	2.59	4.02
G = 2.4 s^{-1}	2.26	2.47	19.70

Discussion

Deep-sea mining activities have great economic potential but come with a high environmental risk (Ramirez-Llodra et al., 2015), which increasingly concerns the sensitized public. The main issue when addressing the potential impacts of mining activities is the present limited knowledge of the biotic and abiotic processes that occur in the abyssal environment and how they will change as a result of mining activities. To predict the long-term, industrial-scale impact of mining activity, numerical modeling techniques are applied. However, the reliability of such models depends on the quality of the input parameters (Jankowski and Zielke, 1997). This study aimed at provid-

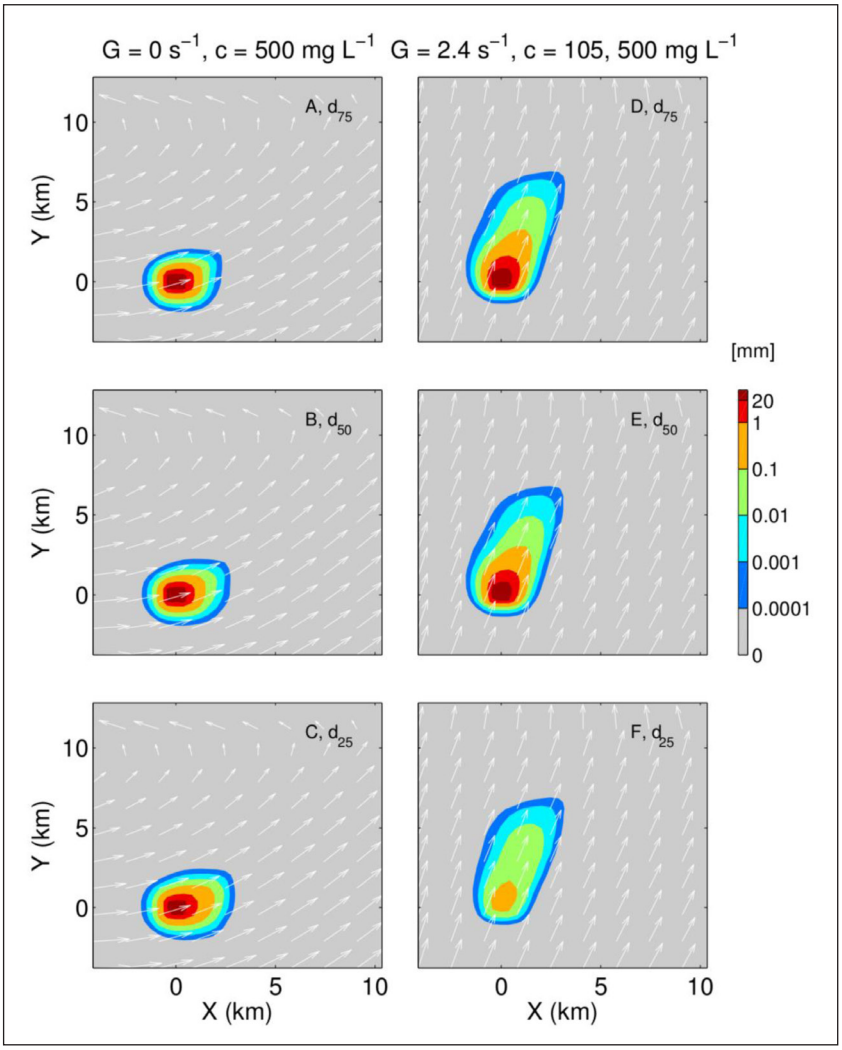

Figure 5: Sediment deposition of plume particles and blanketing of the seafloor. The thickness (mm, color bar scale) of sediment deposition is shown for three particle size classes (d_{25}, d_{50}, and d_{75}) after 4 days of continuous sediment discharge (60 t h^{-1}) 5 m above the seafloor (position 0;0), followed by 1 day of settling at an initial discharge concentration of 500 mg dw L^{-1}. The mean current velocity is shown as arrows that correspond to 3.8 cm s^{-1} in **A**–**C** (low flow; G = 0 s^{-1}) and 10 cm s^{-1} in **D**–**F** (eddy flow; G = 2.4 s^{-1}). DOI: https://doi.org/10.1525/elementa.343.f5

ing a reliable dataset for the behavior of deep-sea particles during the discharge of mining plumes.

Analysis of sediment particle size distribution

Attention should be paid to the location site of the mining activity and the sediments that predominate there. Sedimentological grain sizes in the German nodule license area in the CCZ showed a multimodal size distribution pattern. Sediments from the vast abyssal plain environment generally exhibit a finer grain size (d_{50} = 20 µm), in agreement with the particle size spectrum obtained from several other deep-sea locations (McCave, 1984; Bianchi and McCave, 2000; Thomsen and Gust, 2000). Coarser sediments (d_{50} = 32 µm) were found near seamounts and ridges. Sediment size distribution in the area is controlled by the hydrodynamic regime of the respective environment following the sortable silt theory (McCave et al., 1995). In a higher current velocity field, such as at the base of a seamount or ridge (White et al., 2008), sediment particle selection and sorting result in coarser particle size distribution over time.

Sampled at the side of a large seamount, the sediment core 106 MUC depicted the highest median particle size (d_{50} = 52 µm; **Figure 2**). This site was dominated by larger biogenic deposition (particles > 63 µm) throughout the entire depth of the sediment core, suggesting that biologically derived material predominantly accumulates at this site. To date, no record of size-dependent, particulate organic carbon (POC) content for this study site is available. According to Mewes et al. (2014) and Volz et al. (2018), the total organic carbon (TOC) concentration varies between 0.2 and 0.6 [wt.%] in the German licensed area in the CCZ. Taking into account the generally low sedimentation rate of ca. 5 mm 10^{-3} $year^{-1}$ in the CCZ (Khripounoff et al., 2006), this seamount which rises to a water depth of 2300 m is unlikely to cause elevated biological production at the sea surface but interferes with the deep-sea currents, producing a wake effect (Roden, 1991; Comeau et al., 1995). As seamounts and ridges are considered a hotspot for biodiversity (Samadi et al., 2006; Sautya et al., 2011), they should remain out of the dispersion path of a mining plume.

The plume aggregation process

Discharge simulations of mining-related sediment plumes indicate a rapid flocculation propensity (within 10 to 135 min), resulting in the formation of large aggregates (up to 1100 µm). The analysis of aggregation under differential settling and turbulent shear showed that the sediment plume concentration and the shear rate dictate the behavior of particles in suspension. Increasing the suspended particle concentration up to 500 mg L^{-1} or the shear rate up to 5.6 G (representing a free-stream velocity of ≈0.5 m s^{-1}) promoted aggregate growth, showing that aggregation dominated over breakup. These results corroborate observations reported for laboratory and natural systems (McCave, 1984; Lick et al., 1993; Milligan and Hill, 1998; Manning and Dyer, 1999; Winterwerp, 2002). Flocculation efficiency was found to be rapid (within 10 min) for a sediment plume concentration of 500 mg L^{-1} and a shear rate (G) of 2–10 s^{-1}. Under these hydrodynamic conditions, which can be expected in the wake of a mining vehicle moving at ≈1 m s^{-1}, more than 90% of the primary particles were scavenged within that time. This scavenging would result in rapid clearance of the water column, subsequently limiting the sediment fallout area of the mining activity.

Settling velocities of aggregated plume particles

The residence time of the mining plume in the water column is controlled by the settling velocities of the particles that compose the plume. The present results confirm that size-specific settling velocities of aggregates are regulated by the hydrodynamic conditions during formation. Increasing the shear rate during aggregation significantly increased size-specific settling velocities (Table S3). A similar relationship was reported in previous investigations for different types of sediments (Lick et al., 1993; Manning and Dyer, 1999). Under a negligible shear rate, aggregates that formed under low plume concentrations of 35 mg L^{-1} showed higher size-specific settling velocities than similar-sized particles under higher plume concentrations. The present results indicate that aggregate shape, which is often neglected in modeling equations (Joshi et al., 2014) for computational reasons, may be an important regulating factor of the size-specific settling velocity (**Figure 4A**) resulting in a decrease in effective density, as discussed by Mikkelsen and Pejrup (2000).

The present results revealed that size-specific settling velocities of plume aggregates >100 µm deviate from typical model-based calculations using either Stokes' or Ferguson and Church's (2004) recalculated values for w_s, as shown in **Figure 6**. Few studies have measured deep-sea particle settling velocities quantitatively, but values in the present study appear in the same order of magnitude as those found for organo-mineral aggregates from the benthic boundary layer of the deep sea (Thomsen et al., 2002) and are comparable to those obtained during dredging operations in shallow waters (Smith and Friedrichs, 2011). The average settling velocities reported by Smith and Friedrichs (2011) varied between 70 and

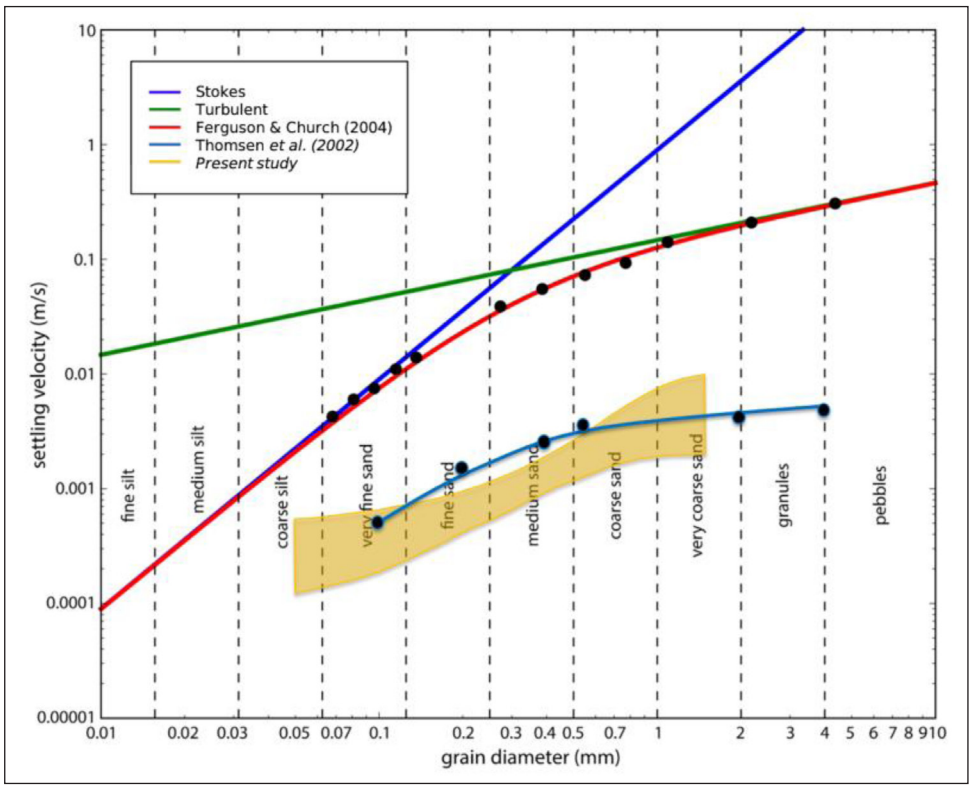

Figure 6: Comparison of settling velocities of measured aggregates with previously published values. Predicted values from Stokes' law and the Ferguson and Church relation are shown with the (lower) measured values from Thomsen et al. (2002) and the present study. Data plotted from the present study relate to the range of settling velocities for all aggregates produced. The figure has been modified from Ferguson and Church (2004). DOI: https://doi.org/10.1525/elementa.343.f6

150 m d^{-1}, while the deep-sea sediments in the present study settled at rates of 88–102 m d^{-1}. The rates may be similar for different reasons, however, given differences between their study and the present study. For example, the largest aggregates in the present study exceeded those in Smith and Friedrichs (2011), as the primary deep-sea sediment particles for aggregation in the present study were smaller (d_{50} = 20 μm; larger aggregates can be formed from smaller particles [Milligan and Hill, 1998]). Samples for the study by Smith and Friedrichs (2011) were also taken from the edge of the plume of the dredged sediments where some features were not representative of the interior of the plume.

Critical shear velocities for resuspension of deposited plume aggregates

The critical shear velocities required to resuspend the aggregates produced in this study are consistent with previously reported values for deep-sea particles (Southard, 1971; Thomsen and Gust, 2000). Once the plume aggregates settled on the seabed, similarities in aggregate resuspension behavior were observed irrespective of their flocculation history. Under a current flow velocity of 3–4 cm s^{-1}, which corresponds to the mean velocity flow in the investigated area (Kuhn, 2015), bedload transport of the plume aggregates starts. These aggregates are expected to accumulate passively between the nodules. Flow velocities >7 cm s^{-1}, which are lower than those encountered during the passage of mesoscale eddies, would potentially yield a new sediment plume of large aggregates.

Sediment plume dispersion modeling

The 5-day mining model prediction reveals a clear variation in the size of the blanketed area depending on the predominant hydrodynamic conditions. The area of influence ranged from 4 km under normal flow conditions to up to 9 km when an eddy passed through the study site. Near-field hyper-sedimentation of >20 mm (**Figure 5**) is expected to drastically impact the deep-sea ecosystem to varying extents (Gollner et al., 2017), which is much less adapted to such events than their counterparts at continental margins (Larsson et al., 2013). In the transitional areas with a decreasing blanketed layer, studies of underwater disposal mining wastes (i.e., dredging, drill cutting [Trannum et al., 2010] and land mining [Smith and Rule, 2001; Hughes et al., 2015]) have shown that instantaneous burial of up to 1 mm does not affect macrofaunal species richness or abundance (Olsgard and Hasle, 1993). However, increasingly divergent communities were observed at a burial rate of 3 mm applied monthly over a period of 6 months (Lohrer et al., 2004). Based on a precautionary approach, we suggest that an ecological blanketing threshold value of around 1 mm should be followed. Such threshold levels can be reached only if restricted, small fallout areas of a few square kilometers with a massive blanketing effect are accepted. These fallout areas will then expand during the passage of mesoscale eddies due to resuspension. However, this plume resuspension would then carry large aggregates, which do not disaggregate into smaller particles unless the shear rate reaches high levels of >5.6 G.

Conclusions

Our findings suggest that the use of elevated sediment discharge (500 mg L^{-1}) under elevated turbulence results in rapid sediment flocculation. The modeling results also suggest that mining under "typical" deep-sea flow conditions results in a relatively rapid deposition of larger particles from the plume, thus restricting the blanketing effect to a smaller fall-out area, unless subsequent flow events resuspend the material. Setting such requirements should therefore be considered for the design of the mining collector and exhaust pipe. Further expansion of this study should consider even higher sediment discharge concentrations and investigate the effect of hindered settling processes (sediment concentration >2–3 g L^{-1}; Winterwerp, 2002) and the gelling effect of cohesive sediment (sediment concentration >30 g L^{-1}; Camenen and van Bang, 2011), which is expected to influence the aggregation and the dispersion potential of the mining plume.

Data Accessibility Statement

Raw data generated during this study have been archived using UC Press Dash under the title of the manuscript (https://doi.org/10.15146/R3K966).

Supplemental files

The supplemental files for this article can be found as follows:

- **Text S1.** Supplemental materials and methods. DOI: https://doi.org/10.1525/elementa.343.s1
- **Tables S1–S8.** Supplemental tables. DOI: https://doi.org/10.1525/elementa.343.s2
- **Figures S1–S7.** Supplemental Figures. DOI: https://doi.org/10.1525/elementa.343.s3

Acknowledgements

The authors would like to thank the shipboard teams and the scientist staff of the RV *Sonne* cruise 240 for the collection of the samples. We are also grateful for the useful proofreading of our manuscript by Candice Thorstenson.

Funding information

We acknowledge BGR Hannover for co-financing this study. B.G. is supported by JPI Oceans2 project "EcoMining-DEU – Ecological Aspects of Deep-Sea Mining". K.P. was supported by the project "Sediment Plume" (FKZ 03F0707B) funded by the German Federal Ministry of Education and Research (BMBF) as part of the Joint Programming Initiative Healthy and Productive Seas and Oceans (JPI Oceans) project "EcoMining-DEU – Ecological Aspects of Deep-Sea Mining". I.M.H. was supported by the Helmholtz Association, the Alfred Wegener Institute Helmholtz Centre for Polar and Marine Research and the DFG-Research Center/Cluster of Excellence "The Ocean in the Earth System" at MARUM. This publication is supported by the HGF Young Investigator Group SeaPump "Seasonal and

regional food web interactions with the biological pump": VH-NG-1000 and by the OceanLab of Jacobs University.

Competing interests

The authors have no competing interests to declare.

Author contributions

- Contributed to conception and design: BG, KP, LT
- Contributed to acquisition of data: BG, KP, AV
- Contributed to analysis and interpretation of data: BG, DC, MIH
- Drafted and/or revised the article: BG, KP, DC, AV, MIH, LT
- Approved the submitted version for publication: BG, KP, DC, AV, MIH, LT

References

Agrawal, YC and **Pottsmith, HC.** 2000. Instruments for particle size and settling velocity observations in sediment transport. *Mar Geol* **168**(1–4): 89–114. DOI: https://doi.org/10.1016/S0025-3227(00)00044-X

Aleynik, D, Inall, ME, Dale, A and **Vink, A.** 2017. Impact of remotely generated eddies on plume dispersion at abyssal mining sites in the Pacific. *Sci Rep* **7**(1): 1–14. Springer US. DOI: https://doi.org/10.1038/s41598-017-16912-2

Amon, DJ, Ziegler, AF, Dahlgren, TG, Glover, AG, Goineau, A, Gooday, AJ, Wiklund, H and **Smith, CR.** 2016. Insights into the abundance and diversity of abyssal megafauna in a polymetallic-nodule region in the eastern Clarion-Clipperton Zone. *Sci Rep* **6**: 1–12. July. Nature Publishing Group. DOI: https://doi.org/10.1038/srep30492

Bianchi, GG and **McCave, IN.** 2000. Hydrography and sedimentation under the deep western boundary current on Bjorn and Gardar Drifts, Iceland Basin. *Mar Geol* **165**(1–4): 137–169. DOI: https://doi.org/10.1016/S0025-3227(99)00139-5

Camenen, B and **van Bang, DP.** 2011. Modelling the settling of suspended sediments for concentrations close to the gelling concentration. *Cont Shelf Res* **31**(10 SUPPL.). DOI: https://doi.org/10.1016/j.csr.2010.07.003

Comeau, LA, Vezina, AF, Bourgeois, M and **Juniper, K.** 1995. Relationship between phytoplankton production and the physical structure of the water column near Coob Seamount Northeast Pacific. *Deep Res* **42**(6): 993–1005. Available at: https://www.sciencedirect.com/science/article/pii/096706379500050G.

Coufort, C, Bouyer, D and **Liné, A.** 2005. Flocculation related to local hydrodynamics in a Taylor-Couette reactor and in a jar. *Chem Eng Sci* **60**(8–9 SPEC. ISS.): 2179–2192. DOI: https://doi.org/10.1016/j.ces.2004.10.038

Drapeau, DT, Dam, HG and **Grenier, G.** 1994. An improved flocculation design for use in particle aggregation experiments. *Limnol Oceanogr* **39**: 723–729. DOI: https://doi.org/10.4319/lo.1994.39.3.0723

Ferguson, RI and **Church, M.** 2004. A simple universal equation for grain settling velocity. *J Sediment Res* **74**(6): 933–937. DOI: https://doi.org/10.1306/051204740933

Fukushima, T. 1995. Overview "Japan Deep-Sea Impact Experiment = JET". *First ISOPE Ocean Mining Symposium*. Tsukuba, Japan: International Society of Offshore and Polar Engineers.

Gollner, S, Kaiser, S, Menzel, L, Jones, DOB, Brown, A, Mestre, NC, van Oevelen, D, Menot, L, Colaço, A, Canals, M, Cuvelier, D, Durden, JM, Gebruk, A, Egho, GA, Haeckel, M, Marcon, Y, Mevenkamp, L, Morato, T, Pham, CK, Purser, A, Sanchez-Vidal, A, Vanreusel, A, Vink, A and **Martinez Arbizu, P.** 2017. Resilience of benthic deep-sea fauna to mining activities. *Marine Environmental Research* **129**: 76–101. Elsevier Ltd. DOI: https://doi.org/10.1016/j.marenvres.2017.04.010

Halbach, P and **Fellerer, R.** 1980. The metallic minerals of the Pacific Seafloor. *GeoJournal* **4**(5): 407–421. DOI: https://doi.org/10.1007/BF01795925

Hein, JR and **Koschinsky, A.** 2013. Deep-Ocean Ferromanganese Crusts and Nodules. In: *Treatise on Geochemistry: Second Edition*, 2nd ed., 273–291. Published by Elsevier Inc. DOI: https://doi.org/10.1016/B978-0-08-095975-7.01111-6

Hill, PS, Boss, E, Newgard, JP, Law, BA and **Milligan, TG.** 2011. Observations of the sensitivity of beam attenuation to particle size in a coastal bottom boundary layer. *J Geophys Res Ocean* **116**(2): 1–14. DOI: https://doi.org/10.1029/2010JC006539

Hughes, DJ, Shimmield, TM, Black, KD and **Howe, JA.** 2015. Ecological impacts of large-scale disposal of mining waste in the deep sea. *Sci Rep* **5**: 1–11. Nature Publishing Group. DOI: https://doi.org/10.1038/srep09985

Iversen, MH, Nowald, N, Ploug, H, Jackson, GA and **Fischer, G.** 2010. High resolution profiles of vertical particulate organic matter export off Cape Blanc, Mauritania: Degradation processes and ballasting effects. *Deep Res Part I Oceanogr Res Pap* **57**(6): 771–784. Elsevier. DOI: https://doi.org/10.1016/j.dsr.2010.03.007

Jackson, GA. 2015. Coagulation in a rotating cylinder. *Limnol Oceanogr Methods* **13**(4): 194–201. DOI: https://doi.org/10.1002/lom3.10018

Jankowski, JA and **Zielke, W.** 1997. Data Support for Modelling of Deep-Sea Mining Impacts. *Seventh Interational Offshore and Polar Engineering Conference* **I**: 451–460. Available at: http://citeseerx.ist.psu.edu/viewdoc/summary?doi=10.1.1.196.1886.

Jones, DOB, Kaiser, S, Sweetman, AK, Smith, CR, Menot, L, Vink, A, Trueblood, D, Greinert, J, Billett, DSM, Arbizu, PM, Radziejewska, T, Singh, R, Ingole, B, Stratmann, T, Simon-Lledó, E, Durden, JM and **Clark, MR.** 2017. Biological responses to disturbance from simulated deep-sea polymetallic nodule mining. *PLoS One* **12**(2). DOI: https://doi.org/10.1371/journal.pone.0171750

Joshi, S, Duffy, GP and **Brown, C.** 2014. Settling velocity and grain shape of maerl biogenic gravel. *J Sediment Res* **84**(8): 718–727. DOI: https://doi.org/10.2110/jsr.2014.51

Kaiser, S, Smith, CR and **Arbizu, PM.** 2017. Editorial: Biodiversity of the Clarion Clipperton Fracture Zone. *Mar Biodivers* **47**(2): 259–264. Marine Biodiversity. DOI: https://doi.org/10.1007/s12526-017-0733-0

Khripounoff, A, Caprais, JC, Crassous, P and **Etoubleau, J.** 2006. Geochemical and biological recovery of the disturbed seafloor in polymetallic nodule fields of the Clipperton-Clarion Fracture Zone (CCFZ) at 5,000-m depth. *Limnol Oceanogr* **51**(5): 2033–2041. DOI: https://doi.org/10.4319/lo.2006.51.5.2033

Klymak, JM and **Legg, SM.** 2010. A simple mixing scheme for models that resolve breaking internal waves. *Ocean Model* **33**(3–4): 224–234. Elsevier Ltd. DOI: https://doi.org/10.1016/j.ocemod.2010.02.005

Kuhn, T. 2015. Low-temperature fluid circulation at seamounts and hydrothermal pits: heat flow regime, impact on biogeochemical processes and its potential influence on the occurence and composition of manganese nodules in the NE Pacific. *SO240/FLUM Cruise Report*. Bundesanstalt für Geowissenschaften und Rohstoffe (BGR). DOI: https://doi.org/10.2312/cr_so240

Larsson, AI, van Oevelen, D, Purser, A and **Thomsen, L.** 2013. Tolerance to long-term exposure of suspended benthic sediments and drill cuttings in the cold-water coral *Lophelia pertusa*. *Mar Pollut Bull* **70**(1–2): 176–188. Elsevier Ltd. DOI: https://doi.org/10.1016/j.marpolbul.2013.02.033

Lick, W, Huang, H and **Jepsen, R.** 1993. Flocculation of fine-grained sediments due to differential settling. *J Geophys Res* **98**(C6): 10279–10288. DOI: https://doi.org/10.1029/93JC00519

Lohrer, AM, Thrush, SF, Hewitt, JE, Berkenbusch, K, Ahrens, M and **Cummings, VJ.** 2004. Terrestrially derived sediment: Response of marine macrobenthic communities to thin terrigenous deposits. *Mar Ecol Prog Ser* **273**: 121–138. DOI: https://doi.org/10.3354/meps273121

Manning, AJ and **Dyer, KR.** 1999. A laboratory examination of floc characteristics with regard to turbulent shearing. *Mar Geol* **160**(1–2): 147–170. DOI: https://doi.org/10.1016/S0025-3227(99)00013-4

Marshall, J, Adcroft, A, Hill, C, Perelman, L and **Heisey, C.** 1997. A finite-volume, incompressible Navier Stokes model for studies of the ocean on parallel computers. *J Geophys Res Ocean* **102**(C3): 5753–5766. DOI: https://doi.org/10.1029/96JC02775

McCave, IN. 1984. Size spectra and aggregation of suspended particles in the deep ocean. *Deep Sea Res* **31**(4): 329–352. DOI: https://doi.org/10.1016/0198-0149(84)90088-8

McCave, IN, Manighetti, B and **Robinson, SG.** 1995. Sortable silt and fine sediment size composition slicing – parameters for paleocurrent speed and paleoceanography. *Paleoceanography* **10**(3): 593–610. Available at: http://apps.isiknowledge.com/InboundService.do?Func=Frame&product=WOS&action=retrieve&SrcApp=Papers&UT=A1995RG33700017&SID=4FoLPHP92OKagaMpJN%2540&Init=Yes&SrcAuth=mekentosj&mode=FullRecord&customersID=mekentosj&DestFail=http%253A%252F%252Faccess.isiprodu. DOI: https://doi.org/10.1029/94PA03039

Mewes, K, Mogollón, JM, Picard, A, Rühlemann, C, Kuhn, T, Nöthen, K and **Kasten, S.** 2014. Impact of depositional and biogeochemical processes on small scale variations in nodule abundance in the Clarion-Clipperton Fracture Zone. *Deep Res Part I* **91**: 125–141. Elsevier. DOI: https://doi.org/10.1016/j.dsr.2014.06.001

Mikkelsen, OA, Hill, PS, Milligan, TG and **Chant, RJ.** 2005. In situ particle size distributions and volume concentrations from a LISST-100 laser particle sizer and a digital floc camera. *Cont Shelf Res* **25**(16): 1959–1978. DOI: https://doi.org/10.1016/j.csr.2005.07.001

Mikkelsen, OA and **Pejrup, M.** 2000. In situ particle size spectra and density of particle aggregates in a dredging plume. *Mar Geol* **170**(3–4): 443–459. DOI: https://doi.org/10.1016/S0025-3227(00)00105-5

Milligan, TG and **Hill, PS.** 1998. A laboratory assessment of the relative importance of turbulence, particle composition, and concentration in limiting maximal floc size and settling behaviour. *J Sea Res* **39**(3–4): 227–241. DOI: https://doi.org/10.1016/S1385-1101(97)00062-2

Nakata, K, Kubota, M, Aoki, S and **Taguchi, K.** 1997. Dispersion of Resuspended Sediment by Ocean Mining Activity -Modelling Study-. *Proceedings of the first International Symposium on Environmental Studies for Deep-Sea Mining*, 169–186. Tokyo, Japan.

Nowald, N, Fischer, G, Ratmeyer, V, Iversen, M, Reuter, C and **Wefer, G.** 2009. In-situ sinking speed measurements of marine snow aggregates acquired with a settling chamber mounted to the Cherokee ROV. *Ocean '09 IEEE Bremen Balanc Technol with Futur Needs*, in press. DOI: https://doi.org/10.1109/OCEANSE.2009.5278186

Oebius, HU, Becker, HJ, Rolinski, S and **Jankowski, JA.** 2001. Parametrization and evaluation of marine environmental impacts produced by deep-sea manganese nodule mining. *Deep Res Part II Top Stud Oceanogr* **48**(17–18): 3453–3467. DOI: https://doi.org/10.1016/S0967-0645(01)00052-2

Olsgard, F and **Hasle, JR.** 1993. Impact of waste from titanium mining on benthic fauna. *J Exp Mar Bio Ecol* **172**(1–2): 185–213. DOI: https://doi.org/10.1016/0022-0981(93)90097-8

Pabortsava, K, Purser, A, Wagner, H and **Thomsen, L.** 2011. The influence of drill cuttings on physical characteristics of phytodetritus. *Mar Pollut Bull* **62**(10): 2170–2180. Elsevier Ltd. DOI: https://doi.org/10.1016/j.marpolbul.2011.07.002

Porter, ET, Sanford, LP, Gust, G and **Porter, FS.** 2004. Combined water-column mixing and benthic boundary-layer flow in mesocosms: Key for realistic benthic-pelagic coupling studies. *Mar Ecol Prog Ser* **271**: 43–60. DOI: https://doi.org/10.3354/meps271043

Ramirez-Llodra, E, Trannum, HC, Evenset, A, Levin, LA, Andersson, M, Finne, TE, Hilario, A, Flem, B, Christensen, G, Schaanning, M and **Vanreusel, A.** 2015. Submarine and deep-sea mine tailing placements: A review of current practices, environmental issues, natural analogs and knowledge gaps in Norway and internationally. *Marine Pollution Bulletin* **97**(1–2): 13–35. Elsevier Ltd. DOI: https://doi.org/10.1016/j.marpolbul.2015.05.062

Ramirez-Llodra, E, Tyler, PA, Baker, MC, Bergstad, OA, Clark, MR, Escobar, E, Levin, LA, Menot, L, Rowden, AA, Smith, CR and **van Dover, CL.** 2011. Man and the last great wilderness: Human impact on the deep sea. *PLoS One* **6**(8). DOI: https://doi.org/10.1371/journal.pone.0022588

Roden, GI. 1991. Mesoscale flow and thermohaline structure around Fieberling seamount. *J Geophys Res* **96**(C9): 16653. DOI: https://doi.org/10.1029/91JC01747

Samadi, S, Bottan, L, Macpherson, E, De Forges, BR and **Boisselier, MC.** 2006. Seamount endemism questioned by the geographic distribution and population genetic structure of marine invertebrates. *Mar Biol* **149**(6): 1463–1475. DOI: https://doi.org/10.1007/s00227-006-0306-4

Sautya, S, Ingole, B, Ray, D, Stöhr, S, Samudrala, K, Kamesh Raju, KA and **Mudholkar, A.** 2011. Megafaunal community structure of Andaman seamounts including the Back-Arc Basin – a quantitative exploration from the Indian Ocean. *PLoS One* **6**(1). DOI: https://doi.org/10.1371/journal.pone.0016162

Serra, T, Colomer, J and **Logan, BE.** 2008. Efficiency of different shear devices on flocculation. *Water Res* **42**(4–5): 1113–1121. DOI: https://doi.org/10.1016/j.watres.2007.08.027

Shen, X. 2016. Modeling Flocculation and Deflocculation Processes of Cohesive Sediments. The College of William and Mary.

Smith, SDA and **Rule, MJ.** 2001. The effects of dredge-spoil dumping on a shallow water soft-sediment community in the Solitary Islands Marine Park, NSW, Australia. *Mar Pollut Bull* **42**(11): 1040–1048. DOI: https://doi.org/10.1016/S0025-326X(01)00059-5

Smith, SJ and **Friedrichs, CT.** 2011. Size and settling velocities of cohesive flocs and suspended sediment aggregates in a trailing suction hopper dredge plume. *Cont Shelf Res* **31**(10 SUPPL.): S50–S63. Elsevier. DOI: https://doi.org/10.1016/j.csr.2010.04.002

Southard, J. 1971. Experimental erosion of calcareous ooze. *J Geophys Res* **76**(24): 5903–5909. Available at: http://onlinelibrary.wiley.com/doi/10.1029/JC076i024p05903/full. DOI: https://doi.org/10.1029/JC076i024p05903

Sternberg, RW, Berhane, I and **Ogston, AS.** 1999. Measurement of size and settling velocity of suspended aggregates on the northern California continental shelf. *Mar Geol* **154**(1–4): 43–53. DOI: https://doi.org/10.1016/S0025-3227(98)00102-9

Sternberg, RW, Ogston, A and **Johnson, R.** 1996. A video system for in situ measurement of size and settling velocity of suspended particulates. *J Sea Res* **36**(1–2): 127–130. Available at: http://www.sciencedirect.com/science/article/pii/S1385110196907820.

Thomsen, L and **Gust, G.** 2000. Sediment erosion thresholds and characteristics of resuspended aggregates on the western European continental margin. *Deep Res Part I Oceanogr Res Pap* **47**(10): 1881–1897. DOI: https://doi.org/10.1016/S0967-0637(00)00003-0

Thomsen, L, VanWeering, T and **Gust, G.** 2002. Processes in the benthic boundary layer at the Iberian continental margin and their implication for carbon mineralization. *Prog Oceanogr* **52**(2–4): 315–329. DOI: https://doi.org/10.1016/S0079-6611(02)00013-7

Trannum, HC, Nilsson, HC, Schaanning, MT and **Øxnevad, S.** 2010. Effects of sedimentation from water-based drill cuttings and natural sediment on benthic macrofaunal community structure and ecosystem processes. *J Exp Mar Bio Ecol* **383**(2): 111–121. Elsevier B.V. DOI: https://doi.org/10.1016/j.jembe.2009.12.004

Van Duuren, FA. 1968. Define velocity gradient model flocculator. *J Sanit Eng Div* **94**(4): 671–682.

Volz, JB, Mogollón, JM, Geibert, W, Arbizu, PM, Koschinsky, A and **Kasten, S.** 2018. Natural spatial variability of depositional conditions, biogeochemical processes and element fluxes in sediments of the eastern Clarion-Clipperton Zone, Pacific Ocean. *Deep Sea Res Part I Oceanogr Res Pap*, 0–1. December 2017. Elsevier Ltd. DOI: https://doi.org/10.1016/j.dsr.2018.08.006

Wedding, LM, Reiter, SM, Smith, CR, Gjerde, KM, Kittinger, JN, Friedlander, AM, Gaines, SD, Clark, MR, Thurnherr, AM, Hardy, SM and **Crowder, LB.** 2015. Managing mining of the deep seabed: Contracts are being granted, but protections are lagging. *Science* **349**(6244): 144–145. DOI: https://doi.org/10.1126/science.aac6647

White, M, Bashmachnikov, I, Arístegui, J and **Martins, A.** 2008. Physical processes and seamount productivity. In: *Seamounts: Ecology, Fisheries and Conservation*, 228–243.

Winterwerp, JC. 2002. On the flocculation and settling velocity of estuarine Mud. *Cont Shelf Res* **22**: 1339–1360. October 2001. DOI: https://doi.org/10.1016/S0278-4343(02)00010-9

Zhu, Z, Wang, H, Yu, J and **Dou, J.** 2016. On the kaolinite floc size at the steady state of flocculation in a turbulent flow. *PLoS One* **11**(2): 1–16. DOI: https://doi.org/10.1371/journal.pone.0148895

How to cite this article: Gillard, B, Purkiani, K, Chatzievangelou, D, Vink, A, Iversen, MH and Thomsen, L. 2019. Physical and hydrodynamic properties of deep sea mining-generated, abyssal sediment plumes in the Clarion Clipperton Fracture Zone (eastern-central Pacific). *Elem Sci Anth*, 7: 5. DOI: https://doi.org/10.1525/elementa.343

Domain Editor-in-Chief: Jody W. Deming, Ph.D., Department of Biological Oceanography, University of Washington, US

Associate Editor: Stephen F. Ackley, B.S., Department of Geological Sciences, University of Texas at San Antonio, US

Knowledge Domain: Ocean Science

Submitted: 16 July 2018 **Accepted:** 07 December 2018 **Published:** 07 January 2019

ELEMENTA Science of the Anthropocene

Elem Sci Anth is a peer-reviewed open access journal published by University of California Press.

OPEN ACCESS